Ultrasonics Sonochemistry 27 (2015) 262–267

Contents lists available at ScienceDirect

Ultrasonics Sonochemistry

journal homepage: www.elsevier.com/locate/ultson

Hysteresis of inertial cavitation activity induced by fluctuating bubble size distribution

Pauline Muleki Seya [a,*], Cyril Desjouy [b], Jean-Christophe Béra [a], Claude Inserra [a]

[a] Inserm, U1032, Lyon, F-69003, France; Université de Lyon, Lyon, F-69003, France
[b] LMFA, Centre Acoustique, Ecole Centrale de Lyon, 69134 Ecully Cedex, France

ARTICLE INFO

Article history:
Received 28 October 2014
Received in revised form 21 May 2015
Accepted 25 May 2015
Available online 27 May 2015

Keywords:
Hysteresis
Inertial cavitation
Bubble size distribution
Acoustic bubble

ABSTRACT

Amongst the variety of complex phenomena encountered in nonlinear physics, a hysteretic effect can be expected on ultrasound cavitation due to the intrinsic nonlinearity of bubble dynamics. When applying successive ultrasound shots for increasing and decreasing acoustic intensities, a hysteretic behaviour is experimentally observed on inertial cavitation activity, with a loop area sensitive to the inertial cavitation threshold. To get a better insight of the phenomena underlying this hysteretic effect, the evolution of the bubble size distribution is studied numerically by implementing rectified diffusion, fragmentation process, rising and dissolution of bubbles from an initial bubble size distribution. When applying increasing and decreasing acoustic intensities, the numerical distribution exhibits asymmetry in bubble number and distribution. The resulting inertial cavitation activity is assessed through the numerical broadband noise of the emitted acoustic radiation of the bubble cloud dynamics. This approach allows obtaining qualitatively the observed hysteretic effect and its interest in terms of control is discussed.

1. Introduction

When looking for technological and acoustical improvements of the therapeutic benefits of ultrasound cavitation, one is led to the problem of understanding the critical process of bubble inception and its effect on the onset of cavitation, as well as overall cavitational effect uncertainties. Indeed ultrasound cavitation is a highly nonlinear phenomenon, sensitive to initial conditions such as the nuclei size and their spatial distribution for instance. At the scale of a single bubble, when driving acoustic intensity is moderate, bubble exhibits classical nonlinear behaviour, such as harmonic generation and resonance frequency shift [1]. For higher acoustic pressures, bubble may undergo non classical nonlinear behaviour, exhibiting period doubling, chaotic oscillations [2] and sonoluminescence [3]. At the scale of the bubble cloud, many nonlinear features also appear, the cloud being a collection of numerous nonlinear oscillators. Multibubble structures have been extensively studied in the aim of many technical and sonochemical applications of ultrasound [4], as well as multibubble sonoluminescence [3]. In particular, insight in the formation of multibubble structures has been provided through a complete spatiotemporal consideration of acoustically driven interacting bubbles [5,6]. Taking advantage of atypical nonlinear effects in underwater acoustics or nonlinear mesoscopic materials [7,8], powerful amplitude-modulated high-frequency waves have shown the possibility of decreasing the onset of cavitation and enhancing cavitation activity through the generation of a low-frequency parametric component [9]. Amongst the variety of complex phenomena encountered in nonlinear physics, such as period doubling, chaos, self-demodulation or memory effects, one can expect to observe hysteretic behaviour of ultrasound cavitation. Usually hysteretic effect result from acoustic energy dissipation induced, for instance, by the presence of microscopic defects such as cracks [10] in geomaterials, interbead contact heterogeneity in granular media [11] or intrinsic nonlinear constitutive stress–strain relationship in soft materials [12]. As peculiar nonlinear signatures are observed for strong acoustic amplitude, the regime in which acoustic bubbles undergo large oscillations leading to bubble collapse, named as the transient or inertial cavitation regime, is more likely to generate nonlinear phenomena. Moreover, in the aim of therapeutic applications, inertial cavitation is commonly considered as the main candidate to explain interaction between ultrasound and cells, leading to cell sonoporation for instance [13,14]. Thus, a full understanding of the inertial cavitation regime, both experimentally and theoretically, is of great importance for improving technological device and the spreading of therapeutic ultrasound. Experimentally, inertial cavitation is characterised by the emission

* Corresponding author.
E-mail address: pauline.muleki@gmail.com (P. Muleki Seya).

http://dx.doi.org/10.1016/j.ultsonch.2015.05.036
1350-4177/

of a broadband noise that has been quantified through an inertial cavitation indicator [15]. More recently the broadband emission has been numerically explained as the consequence of the fluctuation of bubble number and bubble size distribution during sonication time [16]. In [15], a hysteretic effect on the inertial cavitation indicator has been qualitatively observed but neither its origin or its relevance for cavitation-based technology have been discussed. This study focuses on a hysteretic effect on inertial cavitation. This effect, studied experimentally and numerically, results from temporal fluctuation in bubble size distribution. Openings on the real-time control of inertial cavitation during sonication are also discussed.

2. Experimental observations

2.1. Materials and methods

A plane piezoelectric transducer (frequency 501 kHz, diameter 20 mm) is immersed in a degassed water bath (20 L tank, O_2 rate in water between 2.3 and 3.7 mg/L). The transducer is located such as its acoustic axis is vertical and covered by 14 mm of water above its surface (Fig. 1). The transducer, electrically matched to 50 Ω, generates a continuous sinusoidal wave provided by a function generator (HP 33120 A), successively amplified by a variable gain amplifier (AD 603) and a power amplifier (50 dB, 200 W, Adece). The electrical power delivered by the generator is ranged between −12 and 9 dBm, which corresponds to acoustic intensities between 0.1 and 12.8 W/cm^2. The sonicated media is composed of 2 mL of degassed water at ambient temperature placed in a well of a culture plate in polystyrene (12 wells, diameter 20 mm, BD sciences). The sonicated well is located above the transducer and its height is adjusted so that the liquid surface corresponds to a node of the stationary wave field of the irradiated medium. A home-made hydrophone (cutting frequency 10 MHz) realised with a PVDF film (diameter 10 mm) moulded in resin (AY 103, Araldite) is located in the vicinity of the transducer to listen the cavitation noise in the exposed medium. The received signal is amplified (20 dB, NF Electronic Instrument® BX31), digitized (acquisition card PXI-5620, 14 bit resolution, 32 MHz sampling frequency, National Instrument®), transferred to a computer and analysed by Labview® software.

A non-referenced inertial cavitation level is calculated from the hydrophone signal: it is defined as the average level of the instantaneous spectrum in dB within the range of 0.1–7.1 MHz. Before sonication, the reference noise is measured then calculated in the same way when the excitation signal is off. The cavitation index quantifying the inertial cavitation level is determined by the subtraction of the non-referenced inertial cavitation level and the reference noise. It is calculated every 5 ms during sonication. This method is detailed in [17,18].

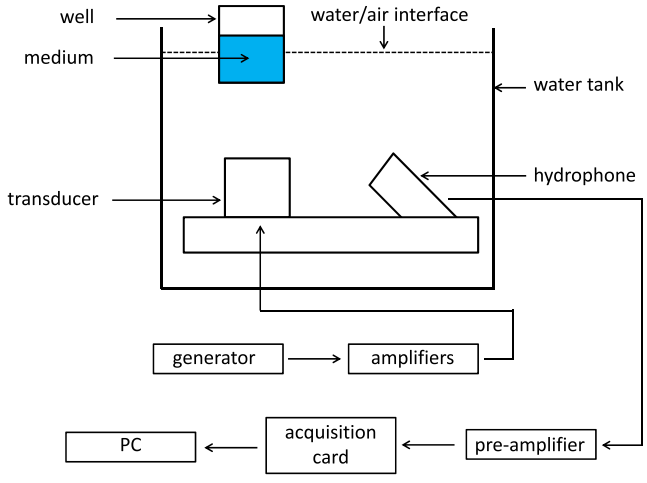

Fig. 1. Experimental setup.

2.2. Results

In order to investigate the hysteresis effects on acoustic cavitation as a function of acoustic intensity, measurements of the cavitation index are performed for increasing and then decreasing acoustic intensity in the same experiment. The protocol of measurements consists of successive ultrasonic excitations separated by times off. Each shot lasts 5 s at a fixed acoustic intensity with a time off between shots fixed to 0.5 s. The acoustic intensity lies in the range 0.1–12.8 W/cm^2 (with up and down logarithmic progression).

Two examples of cavitation index time evolution obtained for increasing and decreasing acoustic intensities are presented on Fig. 2(a) and (b). On these figures, when acoustic intensity increases, the cavitation index sharply increases (solid lines) around the inertial cavitation threshold, 1.3 W/cm^2 in Fig. 2 and 4 W/cm^2 in Fig. 2(b). When acoustic intensity decreases, there is inertial cavitation for acoustic intensities lower than the inertial acoustic threshold obtained for increasing intensities. It is worth noting that inertial cavitation threshold is variable because of the stochastic behaviour of acoustic cavitation. Two spectra calculated from cavitation index shown on the Fig. 2(a) for an acoustic intensity equal to 1.27 W/cm^2 (for increasing and decreasing acoustic intensity respectively) are presented on Fig. 2(c). The broadband noise level for decreasing acoustic intensity is much higher than for increasing acoustic intensity and so is the cavitation index. The broadband noise elevation is accompanied with the apparition of harmonics and subharmonics, ensuring that both stable and inertial cavitation are coexisting for this particular case. The lack of these harmonics and subharmonics on the spectrum corresponding to the increasing path could indicate that ultrasound cavitation is not yet fully initiated, even for the signatures of stable cavitation.

3. Numerical modelling

3.1. Model description

To get insight in the physical phenomena underlying the observed hysteretic loop, the time evolution of the bubble distribution in the medium is simulated. The impact of sufficiently strong acoustic field on the bubble population could modify the radii distribution (by rectified diffusion or fragmentation) but also the spatial location (through primary and secondary Bjerknes forces). For the sake of simplicity, we first focus on the bubble size distribution evolution by considering clouds of non-interactive bubbles. Once the bubble size distributions are obtained for the whole ultrasound protocol, bubble interaction dynamics are taken into account in the computation of the radiated acoustic emission of the bubble cloud in order to estimate the acoustic cavitation noise, following the model of Yasui [16].

For a given bubble size distribution in the medium before ultrasound excitation, fluctuation in this distribution would appear when bubbles experience weak nonlinear oscillations (through rectified diffusion process) or strong nonlinear oscillations and collapses (through fragmentation process), depending on their equilibrium radius R_0 and the applied acoustic intensity I_a. To know which mechanism will act on a bubble for a given couple (I_a, R_0), a map of the cavitation activity is performed by solving the

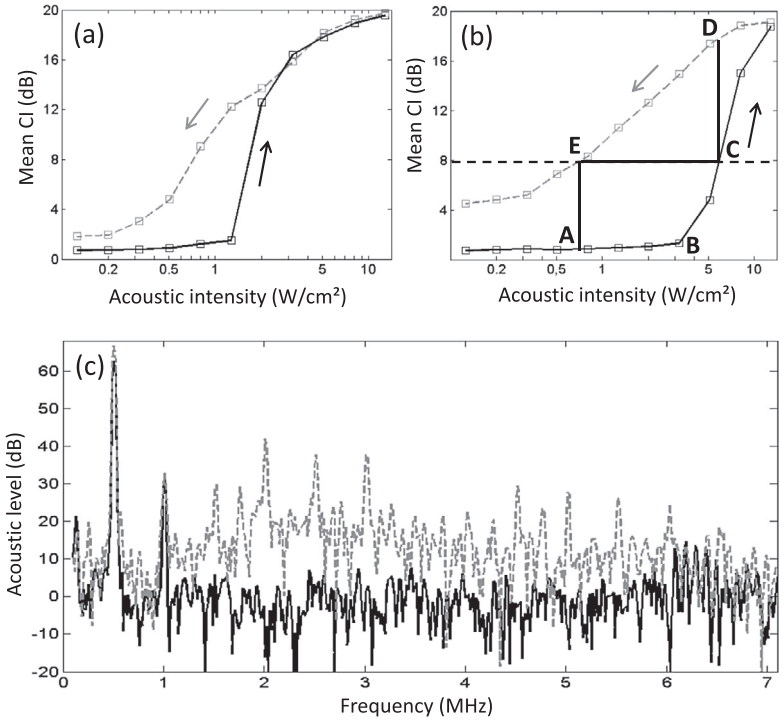

Fig. 2. On (a) and (b), two examples of the hysteresis effect on cavitation index versus acoustic intensity (up with solid line and down with dashed line) and on (c), the spectra corresponding to two measurements for increasing and decreasing acoustic intensity respectively at 1.27 W/cm^2 in (a).

Rayleigh–Plesset equation, assuming polytropic behaviour of gas and neglecting thermal and acoustic dissipation:

$$R\ddot{R}+\frac{3}{2}\dot{R}^2+\frac{4\mu}{\rho R}\dot{R}=\frac{p_v(T_\infty)-[p_\infty-p_{ac}(t)]}{\rho}+\frac{p_g}{\rho}\left(\frac{R_0}{R}\right)^{3\kappa} \quad (1)$$

where R and R_0 are respectively the instantaneous and equilibrium radius of the bubble, p_∞ and T_∞ are the pressure and temperature far from the bubble, p_v is the vapour pressure, κ the polytropic exponent, ρ and μ the liquid density and viscosity, p_g the gas pressure defined by $p_g=p_\infty-p_v(T_\infty)+2\sigma/R_0$, with σ the surface tension. This equation is computed for a sinusoidal acoustic perturbation $p_{ac}(t)=\delta p\sin(2\pi f_{ex}t)$ at the experimental acoustic frequency f_{ex} and for pressure amplitudes δp ranging between 0.1 and 100 bars. The evolution of the normalised maximal bubble radius is shown in Fig. 3 as a function of the acoustic pressure and equilibrium radius. Two areas can clearly be identified depending on the applied acoustic pressure: an area of quasilinear oscillations for low pressure amplitudes below a strongly non-linear area for higher pressure amplitude by a sudden increase in the maximal attained bubble radius. The transition between the two states corresponds to the threshold for which the bubble radius exceeds the commonly used cavitation threshold $R=2.3R_0$, effect which is generally identified as an indicator of inertial cavitation [19].

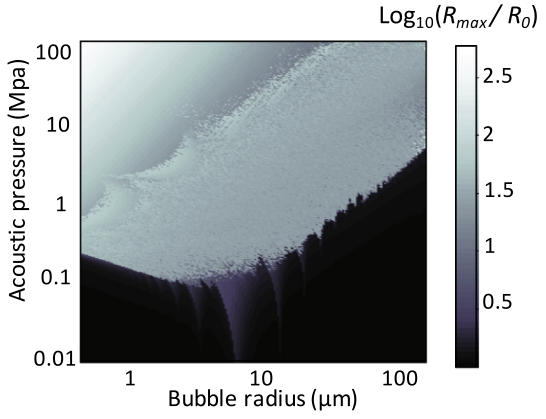

Fig. 3. Variation of the normalised maximum bubble radius (R_{max}/R_0) with initial conditions of bubble radius (0.5 µm to 150 µm) and acoustic pressure (0.1 to 100 bars) at 501 kHz. Logarithmic scale is used for readability.

For a given applied acoustic intensity, bubbles whose cavitational activity remains under the inertial cavitation threshold undergo rectified diffusion effect. Rectified diffusion results from a dissymmetry between gas diffusion inside the bubble during the expansion of the cavity and gas diffusion outside during the contraction of the cavity. In the expansion phase, gas pressure in the bubble decreases and so does the dissolved gas concentration at the bubble wall, according to the Henry's law. When bubble size decreases, the bubble concentration decreases, resulting in an oscillating diffusion flux. The process has a non-zero average, leading to a net gas accumulation in the bubble over one oscillation cycle. The bubble growth, which is noticeable over many acoustic periods, can be described by the evolution of the equilibrium bubble radius [20]:

$$\frac{dR_0}{dt}=\frac{Dd_1}{R_0}\left[\left\langle\frac{R}{R_0}\right\rangle\left(1+\frac{4\sigma}{3P_hR_0}\right)^{-1}\left(\frac{c_i}{c_s}-\frac{\left\langle(R/R_0)^4(P_g/P_h)\right\rangle}{\left\langle(R/R_0)^4\right\rangle}\right)\right] \quad (2)$$

where D is the gas diffusion coefficient, σ is the surface tension, P_h is the hydrostatic pressure, c_i and c_s are respectively the initial and saturated dissolved gas concentration in the liquid and $\langle\rangle$ represents the time-average over an acoustic period. The parameter d_1 and time-average terms are defined in [20].

For bubbles above the inertial cavitation threshold, fluctuation in the bubble size distribution would mainly occur because bubbles collapse in several daughter bubbles. The phenomenon of bubble fragmentation is still misunderstood, and the knowledge of the

number of daughter bubbles is still an open question [21,22], depending on the experimental conditions [22] or vibrating modes of the bubble surface as shown by numerical simulation for which cavitation bubbles are distorted by spherical harmonics [23]. In the present study, as fragmentation of bubbles is a random process, the number of daughter bubbles is determined through a random variable ranging between 2 and 10. This range allows maintaining numerically a sufficient number of bubbles within the medium without lying below the minimal bubble radius. A random variable is assigned to each class of bubble radius at a given step. The size of the bubble is given by mass conservation during fragmentation. The number of bubbles in a given radius class R_a, between step (i) to $(i+1)$ of increasing or decreasing acoustic intensity, will evolve as $n_{R_a}(i+1) = n_{R_a}(i) + \sum n_{R_j}(i) r_j \delta_{1p}$, where n_{R_j} is the number of bubbles in a given class j at the step (i), r_j is a random number determining the number of daughter bubbles after fragmentation of the radius class j, and δ_{1p} equals to 0 or 1 with $p = (R_a/R_j)r_j^3$, meaning that the daughter bubbles issued from the fragmentation process of the class j fall into the bubble class a ($\delta_{1p} = 1$) or not ($\delta_{1p} = 0$).

Between successive acoustic irradiations, cavitation bubbles become free and thus begin to dissolve or rise vertically due to their buoyancy. Concerning dissolution process, Fick diffusion law applied to a bubble in an infinite medium led Epstein and Plesset [24] to derive the bubble free evolution as [25]:

$$\frac{dR}{dt} = \frac{c_s D}{\rho_g}\left(\frac{c_i}{c_s} - 1 - \frac{2\sigma}{RP_h}\right)\left(\frac{1}{R} + \frac{1}{\sqrt{\pi D t}}\right) \tag{3}$$

where ρ_g is the gas density and g is the acceleration of gravity. In parallel, bubbles rising occurs and results from the competition between drag and buoyancy forces. Considering bubbles as empty non oscillating spheres [1], bubbles with radius greater than $\sqrt{3\mu h/g(\rho_l - \rho_g)t_{off}}$ (h being the liquid height, ρ_l the liquid density and t_{off} the duration of the time off between ultrasound shots) at the end of the ultrasound excitation would disappear.

Starting from an initial bubble distribution for degassed water extrapolated from [26], fluctuations of size distribution are computed through the mechanisms described previously when applying increasing–decreasing acoustic intensity. Bubble radii ranged between 0.1 μm and 150 μm with applied acoustic intensities up to 4.17 W/cm^2. For each applied acoustic intensity, the sonication consists in a 5 s excitation followed by a 0.08 s time off. The numerical time off differs from the experimental one in order to avoid bubble disappearance due to the lower boundary of the numerical bubble radius range. Fig. 4 presents an example of the evolution of the bubble size distribution for an upward and downward applied acoustic intensity between 0.17 and 4.17 W/cm^2. It is first noticed that the increase in the acoustic pressure makes the total bubbles number varying up to 10^4–10^5 bubbles in the volume. The influence of the rectified diffusion process modifies the shape of the distribution by promoting the existence of bubbles around the resonant radius (around 6 μm for a 500 kHz excitation). When reaching the maximum acoustic pressure and starting to follow the downward pressure path, fragmentation process results in the enhancement of the asymmetry of the bubble size distribution. It is worth noting that, due to the random behaviour of the fragmentation process included in the numerical model, each bubble size distribution is unique for a given "up and down" pressure sweep. In order to mimic numerically the listening of the cavitation noise and extract the collapsing activity of bubbles such as observed experimentally, the acoustic cavitation noise induced by these bubble size distributions is estimated following the model of Yasui [16]. This model relies on the numerical estimation of the broadband noise emitted by an interacting bubble cloud where the number of bubbles fluctuates. Considering a cloud constituted of uniformly distributed monodisperse bubbles [27], the coupling strength S, characterising bubble's interactions, is inversely proportional to the mean bubble–bubble distance $d_i \cong N_b^{-3/2}$, such as $S = \sum_{i=1}^{N} \frac{1}{d_i}$ for a N_b-bubble cloud. Thus, for a typical bubble number of 10^5 in a 1 cm^3 elementary volume, the coupling strength could reach 10^5. The fluctuation of the coupling strength δS is obtained through the fluctuation in the number of collapsing bubbles between successive ultrasound shots. The temporal evolution of the interaction parameter is then $S(t) = S_m + r\delta S$, where S_m is the mean coupling strength estimated for a given bubble size distribution, and r a random number ranging between 0 and 1 to simulate the random behaviour of bubble nucleation and fragmentation during a sonication. These fluctuations are simulated thanks to Keller–Miksis equation for the bubble dynamics, with a supplementary acoustic source $-S(t)(R^2\ddot{R} + 2R\dot{R}^2)$ characterising multi-bubble interaction for an in-phase oscillating bubble cloud. For each applied acoustic pressure, the temporal evolution of the bubble radius is obtained and the acoustic pressure radiated from the bubble cloud is implemented as

$$P_{em} = S(t)\rho(R^2\ddot{R} + 2R\dot{R}^2) \tag{4}$$

Finally, to simulate the numerical listening of the induced cavitation noise, the acoustic radiated pressure P_{em} is used as an entry of an hydrophone model (second-order low-pass filter of characteristic frequency 5 MHz). Numerical spectrum and cavitation index are obtained using the frequency spectrum of the hydrophone signal, and its mean arithmetic value between 0.1 and 7.1 MHz, at a given acoustic pressure amplitude.

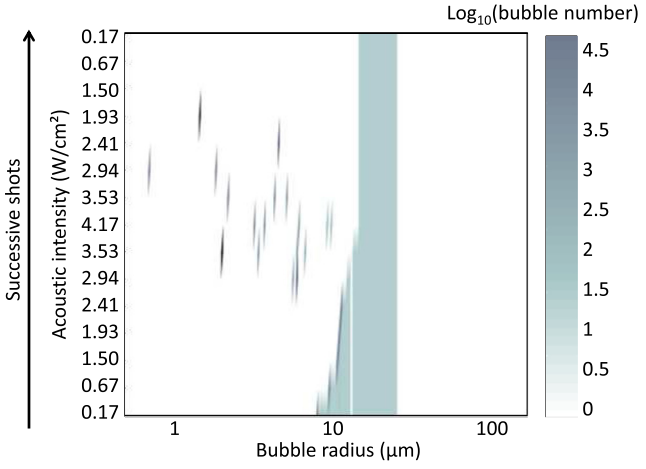

Fig. 4. Bubble size distributions at the end of each shot for increasing–decreasing acoustic excitations.

3.2. Numerical results

Two examples of numerical cavitation index evolutions obtained for increasing and decreasing acoustic pressure are presented on Fig. 5(a) and (b). The hysteretic curve obtained on Fig. 5(a) is the result of the numerical estimation of the broadband noise induced by the fluctuating bubble size distribution shown in Fig. 4. An example of two numerical spectra associated to values given on Fig. 5(a) (acoustic pressure 2.41 W/cm^2 for increasing and decreasing paths respectively) is shown in Fig. 5(c). Around the increasing acoustic intensity of 2.41 W/cm^2, some bubble intervals start collapsing and new daughter bubbles are generated. This results in the fluctuation of the bubble size distribution, both

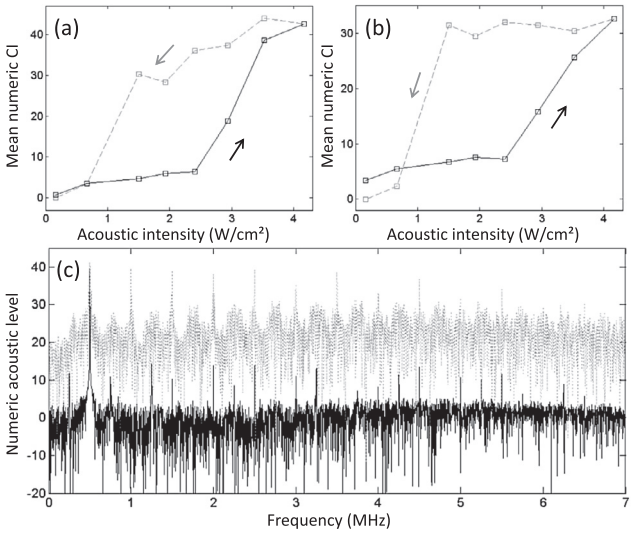

Fig. 5. On (a) and (b), two examples of the hysteresis effect on numerical cavitation index versus acoustic intensity (up with solid line and down with dashed line) and on (c), the spectrum of two measurements for the same acoustic intensity 2.41 W/cm^2 on (a) for increasing and decreasing acoustic intensity respectively.

in terms of total bubble number and bubble size repartition, which increases the interacting behaviour of the bubble cloud. In consequence the broadband noise emerges suddenly and a numerical inertial cavitation threshold appears with a sharp increase of the numerical cavitation index (with a 25 dB dynamics on Fig. 5(b)). It is worth noting that the dynamical range of attained numerical cavitation index is similar to the one observed experimentally. After reaching the maximal acoustic intensity 4.17 W/cm^2, the numerical cavitation index follows a different path for decreasing acoustic intensities leading to higher CI values (than for increasing). These higher CI values result from more important fluctuations in bubble number as the bubble number in the medium reaches its higher value at the maximum applied acoustic intensity, and consequently the highest fluctuation when fragmentation process occurs (Fig. 4). Moreover, the bubble radius after fragmentation is smaller and closer to resonant radius meaning that the acoustic intensity for collapsing is less important (Fig. 3). In consequence, as fluctuation occurs when some bubble radii exceeds the cavitation threshold, smaller bubbles generated by fragmentation process are submitted to more intense fluctuation in their number, even if these small bubbles are below the inertial cavitation threshold and will not experience collapses at this acoustic intensity. A hysteretic loop is obtained, reproducing the hysteretic loop observed experimentally (Fig. 2), at least qualitatively.

This hysteretic behaviour, besides the fundamental interest of the physical phenomenon of cavitation, indicates prospects for future applications of acoustic monitoring and control of inertial cavitation process. Indeed, in therapeutical applications for which moderate cavitation activities are required, such as sonoporation or drug delivery, a main concern is the stochastic behaviour of cavitation process and the inherent variability in cavitation-based biological effects. For example, as shown in Fig. 2(b), sonication at a fixed acoustic intensity (2 W/cm^2 for instance) could generate inertial cavitation activity varying between 1 (no cavitation) and 13 (moderate inertial cavitation activity). As many biological application seem correlated to the inertial cavitation activity, ensuring a given cavitation state would result in a better efficiency of cavitation-based ultrasound applications [28]. When looking at the hysteretic loop ABCDEA on Fig. 2(b), one solution for the maintenance and control of a given cavitation activity (CI = 8 on line CE) is the real-time modulation of the applied acoustic intensity. Indeed, starting from an initial acoustic intensity (0.8 W/cm^2 for point A), reaching the target CI = 8 will require to increase the applied acoustic intensity on the lower branch, until initiating cavitation process after the inertial cavitation threshold (point B). Once cavitation is initiated, the target CI = 8 in point C could easily jump to a higher cavitation state (point D) due to the metastable behaviour of the phenomenon. Following the upper branch by decreasing the applied acoustic intensity would result to come back to the target (point E), before repeating this process in the range of acoustic intensities lying between points A and C. This real-time modulation technique has been the basics of first feedback loop process to control cavitation activity in continuous [17] and pulsed [18] ultrasound sonication. Of interest is the fact that this hysteretic curve appears as the envelope of overall cavitation activity as a function of acoustic intensity used to demonstrate the variability of the process (see Fig. 4 of [17] for instance). As a consequence, this characteristic curve can be used as a calibration measurement in order to define the range of acoustic intensities in which a control process could be performed.

4. Conclusion

A hysteresis effect on cavitation vs acoustic intensity has been observed. This effect is linked to the fluctuations in bubble size distribution during and between each acoustic excitation. The modelling of the evolution of bubble distribution has been simulated by taking into account the main mechanisms involved during sonication (rectified diffusion and fragmentation) and between ultrasound shots (dissolution or rising of bubbles). Numerical spectra calculated from these bubble distributions are used to determined an associated numerical cavitation index. A hysteresis effect on numerical cavitation index as a function of acoustic intensity is found numerically and reproduces qualitatively the one observed experimentally. This hysteresis effect could be used as a calibration curve on acoustic intensity range in order to control acoustic cavitation activity through a modulation of the applied acoustic intensity.

Acknowledgements

This work was supported by the French National Research Agency ANR project "SonInCaRe" (2010-TECS-003-01). It was performed within the framework of the LabEx CeLyA (ANR-10-LABX-0060) of Université de Lyon, within the program "Investissements d'Avenir" (ANR-11-IDEX-0007) operated by the French National Research Agency (ANR).

References

[1] W. Lauterborn, T. Kurz, Physics of bubble oscillations, Rep. Prog. Phys. 73 (10) (2010) 106501.
[2] U. Parlitz, V. English, C. Scheffczyk, W. Lauterborn, Bifurcation structure of bubble oscillators, J. Acoust. Soc. Am. 88 (2) (1990) 1061–1077.
[3] R.F. Young, Sonoluminescence, CRC Press, Boca Raton, FL, 2005.
[4] C. Leonelli, T.J. Mason, Microwave and ultrasonic processing: now a realistic option for industry, Chem. Eng. Process. 49 (2010) 885–900.
[5] U. Parlitz, R. Mettin, S. Luther, I. Akhatov, M. Voss, W. Lauterborn, Spatio-temporal dynamics of acoustic cavitation bubble clouds, Philos. Trans. R. Soc. London A – Math. Phys. Eng. Sci. 357 (1999) 313–334.
[6] R. Mettin, S. Luther, C. Ohl, W. Lauterborn, Acoustic cavitation structures and simulations by a particle model, Ultrason. Sonochem. 6 (1–2) (1999) 25–29.
[7] M.A. Averkiou, Y.S. Lee, M.F. Hamilton, Self-demodulation of amplitude amplitude-modulated and frequency-modulated pulses in a thermoviscous fluid, J. Acoust. Soc. Am. 94 (5) (1993) 2876–2883.
[8] V. Tournat, V.E. Gusev, B. Castagnede, Self-demodulation of elastic waves in a one-dimensional granular chain, Phys. Rev. E 70 (2004) 056603.
[9] B. Gilles, J.C. Bera, J.L. Mestas, D. Cathignol, Reduction of ultrasound inertial cavitation threshold using bifrequency excitation, Appl. Phys. Lett. 89 (9) (2006) 094106.
[10] P. Johnson, A. Sutin, Slow dynamics and anomalous nonlinear fast dynamics in diverse solids, J. Acoust. Soc. Am. 117 (1) (2005) 124–130.

[11] V. Tournat, V.E. Gusev, Acoustics of unconsolidated model granular media: an overview of recent results and several open problems, Acta Acust. United Acust. 96 (2) (2010) 208–224.
[12] T. Divoux, V. Grenard, S. Manneville, Rheological hysteresis in soft glassy materials, Phys. Rev. Lett. 110 (1) (2013) 018304.
[13] J. Sundaram, B. Mellein, S. Mitragotri, An experimental and theoretical analysis of ultrasound-induced permeabilization of cell membranes, Biophys. J. 84 (5) (2003) 3087–3101.
[14] Y. Zhou, J. Cui, C.X. Deng, Dynamics of sonoporation correlated with acoustic cavitation activities, Biophys. J. 94 (7) (2008) L51–L53.
[15] J. Frohly, S. Labouret, C. Bruneel, I. Looten-Baquet, R. Torguet, Ultrasonic cavitation monitoring by acoustic noise power measurement, J. Acoust. Soc. Am. 108 (5) (2000) 2012–2020.
[16] K. Yasui, T. Tuziuti, J. Lee, T. Kozuka, A. Towata, Y. Iida, Numerical simulations of acoustic cavitation noise with the temporal fluctuation in the number of bubbles, Ultrason. Sonochem. 17 (2) (2010) 460–472.
[17] A. Sabraoui, C. Inserra, B. Gilles, J.-C. Béra, J.-L. Mestas, Feedback loop process to control acoustic cavitation, Ultrason. Sonochem. 18 (2) (2011) 589–594.
[18] C. Desjouy, A. Poizat, B. Gilles, C. Inserra, J.-C. Béra, Control of inertial acoustic cavitation in pulsed sonication using a real-time feedback loop system, J. Acoust. Soc. Amer. 134 (2) (2013) 1640–1646.
[19] T. Leighton, The Acoustic Bubble, Academic Press, 1994.
[20] L.A. Crum, Measurements of the growth of air bubbles by rectified diffusion, J. Acoust. Soc. Am. 68 (1) (1980) 203–211.
[21] H.G. Flynn, A mechanism for the generation of cavitation maxima by pulsed ultrasound, J. Acoust. Soc. Am. 76 (2) (1984) 505–512.
[22] W. Lauterborn, Cavitation bubble dynamics – new tools for an intricate problem, Appl. Sci. Res. 38 (1982) 165–178.
[23] C.E. Brennen, Fission of collapsing cavitation bubbles, J. Fluid Mech. 472 (2002) 153–166.
[24] P. Epstein, M. Plesset, On the stability of Gaz bubbles in liquid–gas solutions, J. Chem. Phys. 18 (11) (1950) 1505–1509.
[25] E.A. Neppiras, Acoustic cavitation, Phys. Rep. – Rev. Sect. Phys. Lett. 61 (3) (1980) 159–251.
[26] C.E. Brennen, Cavitation and Bubble Dynamics, Oxford University Press, Oxford, 1995.
[27] Y. Kai, M. Maimaitiming, Z.C. Ying, Z.Q. Rong, A. Yu, Observing multi-bubble sonoluminescence in phosphoric acid, in: Nonlinear Acoustics State-of-the-Art and Perspectives (ISNA 19), AIP Conference Proceedings, vol. 1474, 2012, pp. 104–111.
[28] C.C. Coussios, R.A. Roy, Applications of acoustics and cavitation to noninvasive therapy and drug delivery, Annu. Rev. Fluid Mech. 40 (1) (2008) 395–420.